Journal of Radioanalytical and Nuclear Chemistry (2024) 333:1883–1897
https://doi.org/10.1007/s10967-024-09388-8

Insight into adsorption behavior of activated ZrO_2 prepared by solution combustion for the removal of chromium and barium ions from aqueous solutions

Maha A. Youssef[1] · Abeer El-khalafawy[1] · Hisham S. Hassan[2]

Received: 24 October 2023 / Accepted: 17 January 2024 / Published online: 24 February 2024

Abstract

The prepared activated zirconium oxide was characterized using different analytic techniques and investigated as a new inorganic sorbent to get rid of the chromium and barium ions from the waste stream. Several experiments have been performed, including the impact of contact time, pH, initial ion concentration, temperature, desorption, and the effect of interfering ions. Different isotherm kinetic models were investigated. The outcomes demonstrated that, the second-order kinetic model was appropriate, and the monolayer capacities for the chromium and barium ions were 35.9 and 33.9 mg/g, respectively. Finally, zirconium oxide was recommended to be used as a highly selective adsorbent for hazardous metal ions.

Graphical abstract

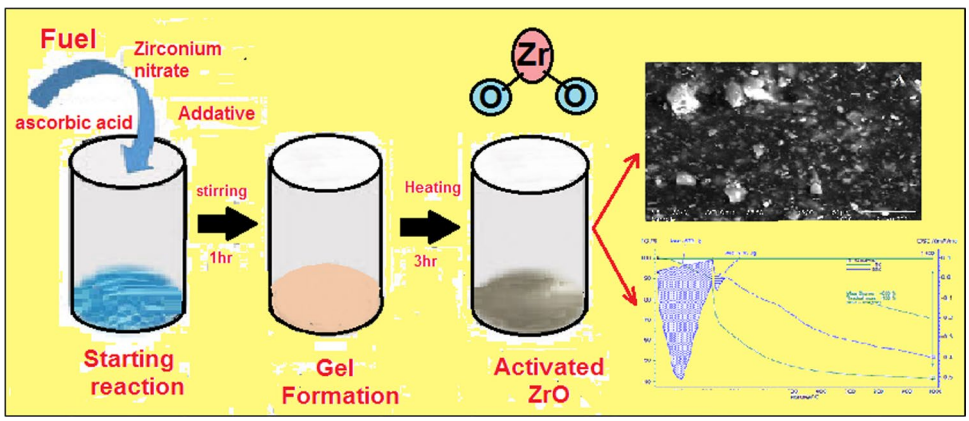

Keywords Adsorption · Chromium · Barium · Activated zirconium oxide

Introduction

The contamination of waste water resources has been a notable concern in worldwide [1]. The most important reason for exposure to toxic metals such as barium and chromium ions is their discharge into the water streams due to the devolution of industrialization in many countries worldwide [2]. The contaminated waste waters caused by the hazardous wastes released into the environment pose a serious threat to the environment and a sizable risk to human health [3]. Furthermore, the contaminated elements have an essentially

✉ Abeer El-khalafawy
abeerelkhalafawy@yahoo.com

[1] Analytical Chemistry and Control Department, Hot Laboratories Center, Egyptian Atomic Energy Authority, Cairo 13759, Egypt

[2] Waste Management Department, Hot Laboratories Center, Egyptian Atomic Energy Authority, Cairo 13759, Egypt

toxic characterization because they are not biodegradable, they are classified as hazardous elements. Therefore, there is a lot of care paid to removing these elements and keeping their concentrations within the permitted limits [4]. Barium ions are considered an element that displays high solubility in water; this phenomenon leads to illimitable mobility in the environment. Radioactive barium is a long-lived radionuclides (^{133}Ba, for example, has a half-life of 10.54 years), which can be produced by a variety of activities, including inadequate radioactive waste management and disposal efforts, unintentional environmental radioactive chemical releases, nuclear practices, and nuclear fuel cycle processes. Exposure to barium ions may cause many health issues, for example, kidney and heart failure, respiratory paralysis, and gastric hemorrhage etc. [5–7]. Recently, many people worldwide were affected by chromium, which polluted water streams. Chromium ions can reach groundwater mostly during anthropogenic activities such as ore refining, electroplating, and leather tanning [8]. The permissible limits of total chromium ion in drinking water must be lower than 0.1 mg/l, and for the various industrial effluents, it must be less than 1.71 mg/l on average per month, according to the United States Environmental Protection Agency. However, the total chromium ion concentrations in some industrial effluents, such as those from the tannery sector, can range from 0.7 to 345 mg/l [9]. Also, chromium species may also be produced during the chemical decontamination process used to remove the oxide layer that has built up in a nuclear power plant's primary system. Additionally, radioactive wastewater has been discovered to contain radioactive chromium (^{51}Cr, $t_{1/2}$ = 27.7 days), which is a result of many nuclear operations such as radioisotope synthesis and radiochemistry research [10]. The most commonly applied techniques for removing dangerous metals from wastewater are reverse osmosis [11], coagulation [12], precipitation [13], ion exchange [14, 15], membrane [16], evaporation [17], adsorption [18, 19], as well as solvent extraction [20]. The adsorption technique is the most widely applied method for removing contaminating materials from wastewater [5], because of its effectiveness [6], and simplicity [7]. Oxides such as silica [24], nanoparticles [25], magnetic materials [26], or composite materials [27] were used in several studies to remove hazardous materials from waste water [28]. So, several studies aim to create novel adsorbents with high adsorption capacities. An inert oxide material called zirconium oxide has great chemical resistance to acids, bases, oxidants, and reductants [29]. With a focus on removing various cations from waste water, metal oxide surface preservation using active molecules has been widely used. In the current study, solution combustion was effectively used to prepare zirconium oxide, which was then used as adsorbent materials for the removal of Cr (III) and Ba (II) from waste water. The preparation method, physico-chemical characterization of the synthesized zirconium oxide powder, and explanation of adsorption were the focus of the studies.

Experimental

Chemicals and reagents

The reagents used in our preparative step are: (1) zirconium nitrate ($Zr(NO_3)_4$), M = 231.22 g/mol, Merck; (2) ascorbic acid $C_6H_8O_6$ (known as vitamin C) with 99.5% purity and M = 176.12 g/mol. Finally, (3) ammonium chloride (NH_4Cl, CAS Number 12125-02-9 from Sigma-Aldrich, USA), M = 53.4913 g/mol. All the reagents used in the second stage of the batch study are of analytical grade and were used without any additional purification. 1000 mg/l of adsorbate stock solutions being prepared by dissolving appropriate metal salts in double distilled water. The salts employed were barium chloride ($BaCl_2$) and chromium oxide salt (Cr_2O_3). The stock solutions were diluted with distilled water to obtain standard solutions.

Preparation and characterization

Generally, solution combustion is a versatile, simple, and rapid process that involves a self-sustained reaction in a homogeneous solution of oxidizers (zirconium nitrates) and fuels (ascorbic acid). The investigation of the low-temperature reaction of ascorbic acid (as a fuel) with zirconium nitrate (as an oxidizer) can be recognized as the starting point for the solution combustion method. These materials are in a solid state at room temperature and have a complex crystal structure. The crystal structure of these compounds contains atoms that function as fuel (H, C) as well as atoms of oxidizer (e.g., O), which are separated by angstrom-scale distances. The reaction of ascorbic acid with zirconium nitrate occurs in air at relatively low temperatures, yielding ultrafine ZrO_2 and a large amount of gaseous products. For example, the reaction of the formation of ZrO_2 can be represented as follows:

$$C_6H_8O_6 + Zr(NO_3)_4 \rightarrow ZrO_2 + 6CO_2 + 4H_2O + 2N_2 \quad (1)$$

Zirconium oxide powder was prepared as follows: A certain amount of $Zr(NO_3)_4$ (7.5 g) and 0.49 g of $C_6H_8O_6$, as well as a definite quantity of NH_4Cl (0.1 g), were dissolved in a specific volume (50 ml) of methanol with stirring for 1 h. The nitrate works as an oxidizer, while the $C_6H_8O_6$ and methanol act as fuels. The mixture was protected in the dark for about 3 days with stirring until the color of the solution changed to a light brown. The zirconium salt was reacted with ascorbic acid and methanol to generate a colored compound.

The solution, after mixing the reactants, was heated in a 100 ml ceramic crucible. The combustion process of the mixture began after 30 min and was accompanied by an explosion sound. The combustion process continued for about 3 h. The product is left to cool at room temperature overnight. After this step, the sample powder has a gray-white color.

Adsorption studies

Different experiments were carried out under kinetic and equilibrium conditions. To specify the pH range at which the maximum adsorption of Cr (III) and Ba(II) on the prepared zirconium oxide occurs, a series of 50 ml test glasses, each including the activated zirconium oxide and 10 ml of a desired concentration (50 mg/L) of two ions, were added to 0.1 g of the prepared material. The mixture of solutions was shaken at room temperature. The different concentrations (50–500 mg/l) were studied. The pH was adjusted to values ranging from 2.0 to 6.0 using a dilute solution of HCl or NaOH. The samples were centrifuged (after a certain period of time) to separate two phases (solid phase and liquid phase), and then a certain volume (5 ml) of the clear liquid phases obtained was pipetted out. The concentrations of ions were determined by the ICP (OES) 6 Wentworth Drive, Hudson New Hampshire 03051, USA. All experiments were conducted in triplicate under the same conditions. The removal percentage ($R\%$), adsorption capacity (q_e, mgg^{-1}), and distribution coefficient (K_d) of Cr(III) and Ba(II) were determined as follows:

$$R\% = \left(\frac{C_0 - C_e}{C_0}\right) \times 100 \tag{2}$$

$$\mathbf{q_e} = (C_0 - C_e)\left(\frac{V}{M}\right) \tag{3}$$

$$K_d = \left(\frac{C_0 - C_e}{C_e}\right)\frac{V}{m} \tag{4}$$

where C_0 and C_e are the initial and equilibrium concentrations (mg/l) of metal ions in solution, respectively, the amount of the studied metal ions retained in the activated zirconium oxide powder is q_e (mg/g), V is the volume (l), and m is the mass (g) of the activated zirconium oxide.

Barium and chromium desorption

The regeneration process can be done by using desorbing agent that results in the greatest percentage of Cr (III) and Ba (II) desorption from the loaded samples under evaluation. To follow the adsorption process, the loaded samples were shaken for 180 min at 25 °C while being in contact with 10 mL of 0.1 M HCl, NaOH, and distilled water. It was done to separate and evaluate the liquid phase. An equation was used to determine the desorption process (5).

$$\text{Desorption } \% = \frac{\text{Amount of desorped ion}}{\text{Amount of adsorped ion}} \times 100 \tag{5}$$

Results and discussion

Characterization of activated zirconium oxide

The technique of x-ray diffraction (XRD) is an important analysis technique used to identify the phase structure of solid samples. An XRD pattern of activated zirconium oxide is presented in Fig. 1. The broad hump was detected at $2\Theta \sim 25°$, conformable to the amorphous nature of activated zirconium oxide [29, 30]. This broad hump may be due to zirconium oxide and hydrocarbon compound hydrogen bonding [31, 32].

The FT-IR spectra of prepared activated zirconium oxide were studied before and after the adsorption of both Cr (III) and Ba (II) to illustrate the different function groups that are responsible for the adsorption process and the changes in activated zirconium oxide after the adsorption process. Infrared analysis was applied to determine the main groups of the activated zirconium oxide, which are clarified in Fig. 2. Essentially, in the amorphous activated zirconium oxide, the FTIR spectra mostly contain –OH groups. These groups ordinarily form a chemical bond with Zr–OH on the material surface [29]. The broad band of –OH stretching vibration is appearing at 3435.62 cm^{-1}; there is a signature for the accompanying stretching amine group ($N–H_2$) with a small band around 3430 cm^{-1} [32]. The stretching vibration of charged amine ($N–H^+$) appears with a band at 2925.53 cm^{-1} while the bending vibration of the amine ($N–H_2$) group appears at 1631.99 cm^{-1}. The symmetric stretching absorption band of C-H is appearing around 2856.79 cm^{-1}. The bending vibration band of the hydrogen attachment with the aromatic ring is appearing at 464.50 cm^{-1}. The absorption bands appearing at 1454.26 and 1385.62 cm^{-1} belonged to (CH_2) bending and (CH_3) symmetrical deformations, respectively. The band displayed at 1098.37 cm^{-1} is assigned to asymmetric stretching of the C–O group [29]. The band at 519 cm^{-1} corresponds to vibrations of the Zr–O bond [33]. It is clear that the peaks changed after the adsorption of two ions due to the interaction and formation of a chemical bond between the ions and the prepared material. As there is a single pair of electrons that can be obtained from the nitrogen atom, the presence of amino groups in the activated zirconium oxide supplies the active sites for the various ions. This behavior of the material could be efficiently applied to

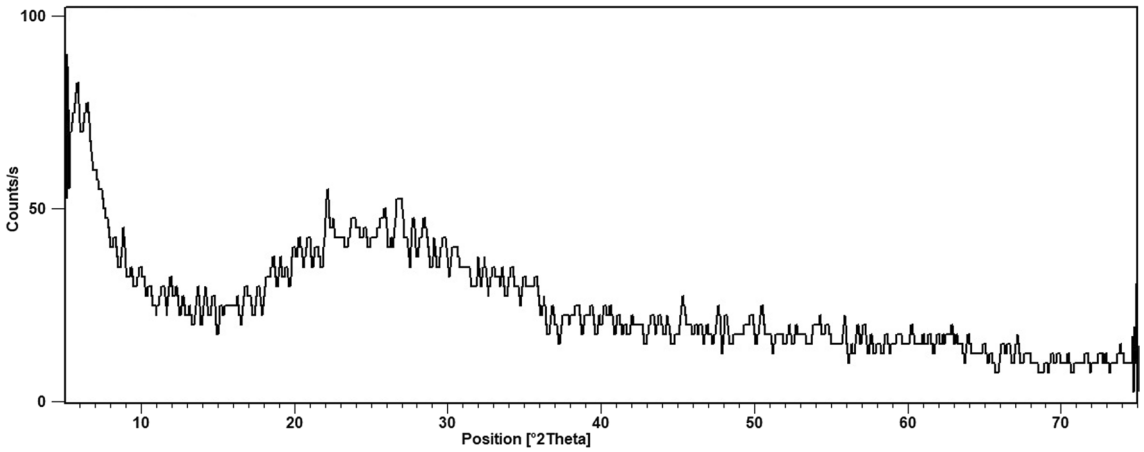

Fig. 1 XRD Pattern for activated zirconium oxide

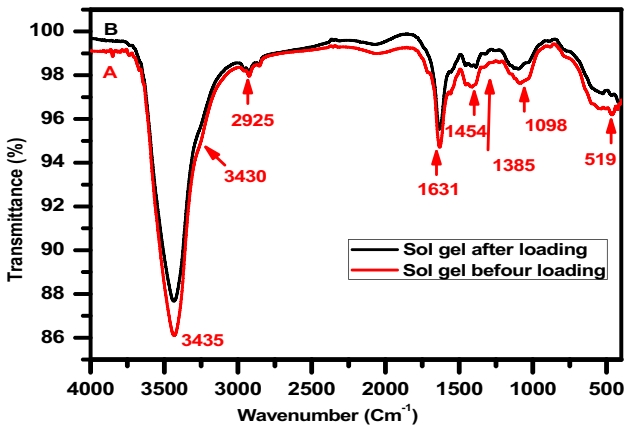

Fig. 2 FT-IR spectrum of, **a** activated zirconium oxide composite, **b** Loaded ZrO_2 by both Cr(III) and Ba(II)

the chelating with Cr (III) and Ba (II)) and the removal of these ions from the waste stream.

SEM micrographs of the activated zirconium oxide were assessed before and during the adsorption of two ions, and the results are shown in Fig. 3. It is clear that the activated zirconium oxide has irregularly agglomerated particles, and the surface of the activated zirconium oxide is rough [29]. A porous and rough surface of activated zirconium oxide was observed; these conditions might favor the adsorption of Ba (II) and Cr (III). The formation of a small granule was observed, and the particle size ranged from 10 μ m to less than 1 μ m. After the adsorption process is completed, some pores are shown to be closed by ions in Fig. 3B.

Activated zirconium oxide's thermal stability was examined using differential scanning calorimetry (DSC) and thermogravimetric. analysis (TGA) (Simultaneous Thermogravimetric, model STA 449 F1 Jupiter, Netzch). The heating of about 10 mg of zirconium oxide powder in an alumina crucible in an inert and oxidative environment was done. Figure 4 shows the DSC data and corresponding TGA data for the melting behavior of the sample powder. The activated zirconium oxide shows decomposition occurring in two stages. The first step, accompanied by weight loss up to 100 °C, coexists with a strong endothermic peak that is attributed to the water rising from the surface [31]. The sample exhibited a total weight loss of 58.63%, with the second stage of weight loss occurring between 200 and 250 °C. Additionally, an endothermic peak was observed in the DSC curve. This is related to the evaporation process of high molecular weight organic compounds that takes place at higher temperatures than the preparation temperature [32].

The pore size distribution and porosity, as well as the specific surface area of the ZrO_2 powders, were determined using the mercury intrusion porosimetry technique with the

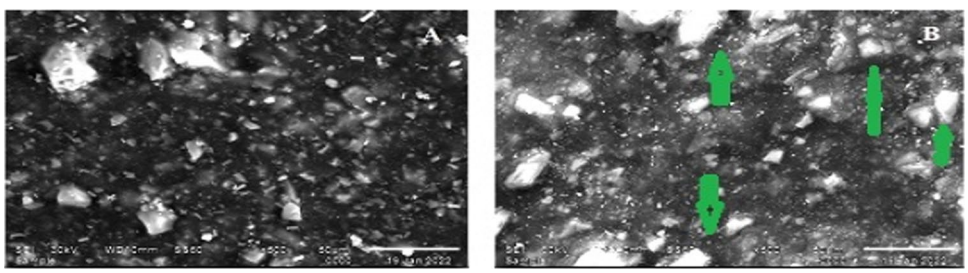

Fig. 3 SEM micrograph of, **A** Activated zirconium oxide, **B** Zirconium oxide loaded with Cr(III) and Ba(II)

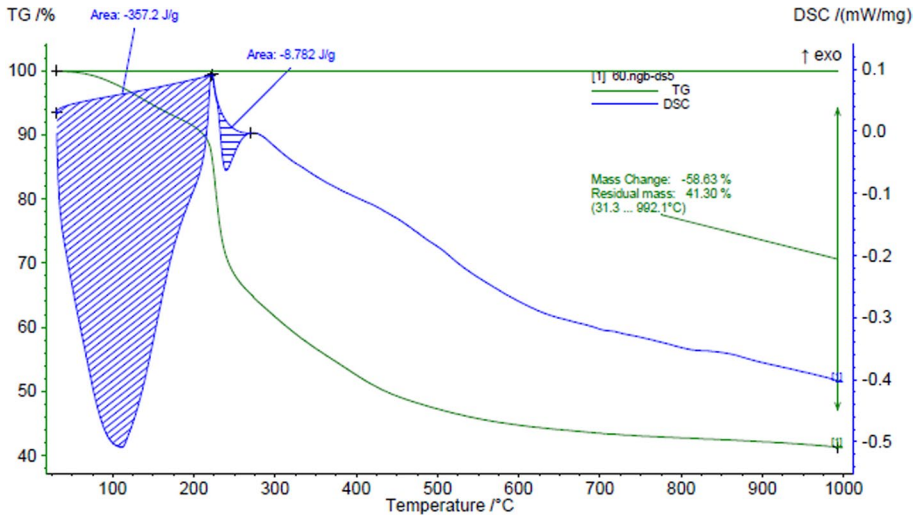

Fig. 4 Thermal analysis results for the activated zirconium oxide: DSC and TGA curves

Table 1 Total specific surface area and porosity of the prepared samples

Sorbent	Specific surface area (m^2/g)	Average pore diameter (nm)	Bulk density (g/mL)	Apparent density (g/mL)	Porosity (%)
ZrO_2	124.21	678	0.54	0.94	92.43

aid of the pore sizer chromatech 9320 (USA). The obtained data is displays in the following Table 1

Effect of pH

The distribution coefficient (K_d) quantities of Cr(III) and Ba(II) onto activated zirconium oxide alter as a function of pH, as shown in Fig. 5A and B, as well as the effect of pH on the removal efficiency of the ions utilized, Cr(III) and Ba(II). From Fig. 5B, it is obvious that the K_d amount increases with the raising of pH values. At highly acidic mediums (lower pH values), the K_d values of Cr (III) and Ba (II) were inhibited; this can be explained as follows: when the pH has a small value, there is an excess of protons that compete with both ions in the aqueous medium and, preferably, seize the active sites available on the surface of the activated zirconium oxide. By raising the pH values, it was observed that the K_d values increased; this may be due to the decrease in proton competition. As can be seen from the figure, Cr(III) has higher K_d values than Ba(II). This is explained by the fact that Cr(III) can diffuse through the sorbent material's surface, allowing ions to occupy a greater number of active sites than Ba(II). The reason for this is because Cr (III) has a lower ionic radius than Ba (II), which makes it easier for Cr (III) to enter the pores on the surface of the sorbent material. Both of the investigated ions have precipitated at higher pH values, making it more challenging to distinguish between the quantity of precipitated ions and the amount of Cr (III) and Ba (II) that adsorbed onto the activated zirconium [6]. This is confirmed by studying the point of zero charge of the prepared adsorbent in Fig. 5C, which displays a relation between the initial pH (pHi) and ΔpH, which is the difference between the final and initial pH values. The point at which the value of pHi is equal to pHf (ΔpH = 0) was recorded as pHpzc. The point of zero charge, pHpzc, can be defined as the point at which the net charge of the surface is zero; higher than this value, the surface charge was negative, and below this value, the surface charge was positive. The lower value of pHpzc indicates that the material is a good sorbent material since it has a wide range of pH values at which the surface has a negative charge; hence, it can attract cations in a wide range of pH values.

The speciation was executed using Hydra/Medusa chemical equilibrium software at a 50 mg/l initial metal ion concentration, room temperature, and a pH range of 1.0–12.0. From the speciation diagram in Fig. 5E and D, the trivalent species, Cr(III), is the predominant species at pH 5 and up to pH 7. Above this value, the chromium ion is precipitated as $Cr(OH)_2$. Therefore, the total chromium removal at a pH lower than 7 is mainly attributed to the sorption process, while the precipitation process is the major mechanism at a pH higher than 7. While for barium ions, the divalent species, Ba^{2+}, is the dominant species till pH 5, it starts to precipitate as $Ba(OH)_2$ species at pH above 5, as displayed in Fig. 5D. pH 5.0 for both cations was selected as the optimum pH value for sorption in order to avoid the precipitation of metal ions in the form of their hydroxides.

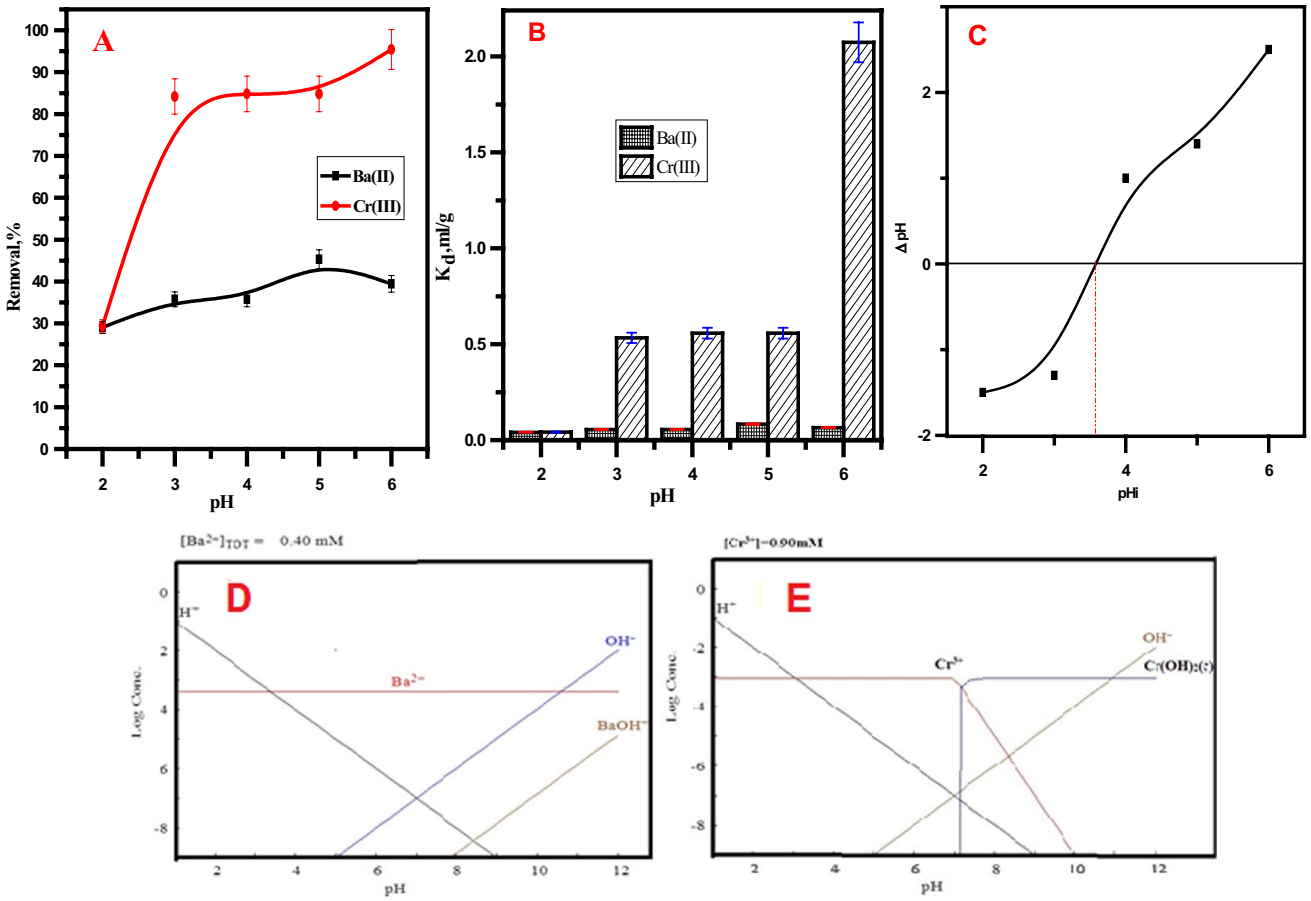

Fig. 5 **A** Effect of pH on the % removal of Cr(III) and Ba(II), **B** Effect of pH on the distribution coefficient(K_d) onto activated zirconium oxide, **C** Point of zero charge(PZC) of activated zirconium oxide, **D** and **E** speciation of Ba(II) and Cr(III), respectively ($Ci = 50$ mg/l, $V = 10$ ml, $m = 0.1$ g, shaking time = 2 h)

Effect of contact time

Exploratory studies regarding the adsorption of both Cr (III) and Ba (II) onto the synthetic activated zirconium oxide within the first 60 min demonstrated the rapid ion adsorption; following this time, adsorption behavior slows down until reaching equilibrium (Fig. 6). This behavior can be explained by the presence of available sites on the surface of zirconium oxide, which have progressively saturated over time. This leads to a decreasing rate of adsorption as equilibrium approaches. The driving force of the adsorption process is the concentration variation between the solid–liquid interface and the bulk solution; at the initial stage, this difference is high, so the adsorption rate becomes high. The adsorption process becomes slower after a period of time; this may be attributed to the slower prevalence of both ions inside the pores at the interface of zirconium oxide. This leads to the ions occupying the available exchangeable sites at the interface of zirconium oxide.

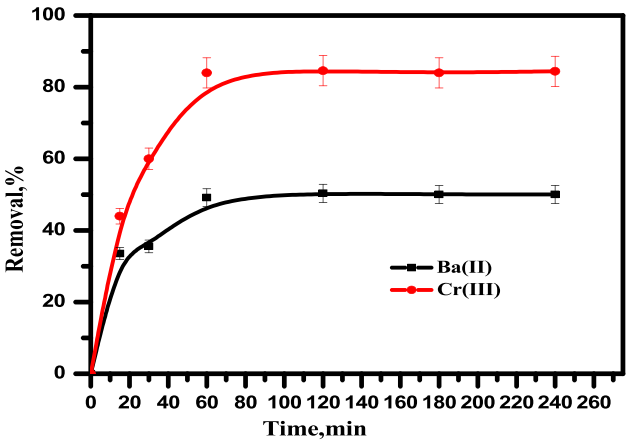

Fig. 6 Effect of contact time on the % removal of Cr(III) and Ba(II) onto activated zirconium oxide ($Ci = 50$ mg/l, $V = 10$ ml, $m = 0.1$ g, pH = 5)

Sorption kinetic modeling

The kinetics model study of the adsorption process has a significant role in knowing the adsorption rate as well as evaluating the most convenient conditions for different applications [34]. The kinetic models of Cr (III) and Ba (II) adsorption onto activated zirconium were studied using four different kinetic models: non linear pseudo-first order; non linear pseudo-second order, linear intra-particle diffusion, and non linear Elovich models. The non-linear equation of the pseudo first-order model can be written as follows [35]:

$$q_t = q_e(1 - e^{-k_1 t}) \tag{6}$$

The quantities of Cr (III) and Ba (II) adsorbed on activated zirconium oxide at equilibrium and at any time (t) are denoted by the symbols q_e and q_t (mg/g), respectively, where k_1 is rate constant of the pseudo first- order model (min^{-1}). Figure 7 clarifies the relationship between the amount of ions adsorbed (q_t) and time (t). The parameters of pseudo first-order (k_1 and q_e) can be assessed, and the data are exhibited in Table 1, as are the values of R^2. The results gained from the pseudo first-order model curve point out the applicability of this model to fit the obtained data through the initial steps for the adsorption of both studied ions. Also, the calculated values of (q_e) must be in agreement with the values of experimental capacities. The data in Table 2 show that the values of the correlation coefficients (R^2) for the plots are good, but the values of the calculated amount adsorbed (q_e) are not in concurrence with the experimental amount (q_e) for Cr(III) and Ba(II). So, it is clear that the adsorption processes of Cr (III) and Ba(II) onto activated zirconium oxide do not follow this model.

The non-linear form of the pseudo-second-order equation is represented by Eq. 6 [34, 35]:

$$q_t = \frac{k_2 q_e^2 t}{1 + k_2 q_e t} \tag{7}$$

k_2 represented the rate constant of pseudo second-order (g/mg min). The relation between the q_t with time, t, for Cr (III)

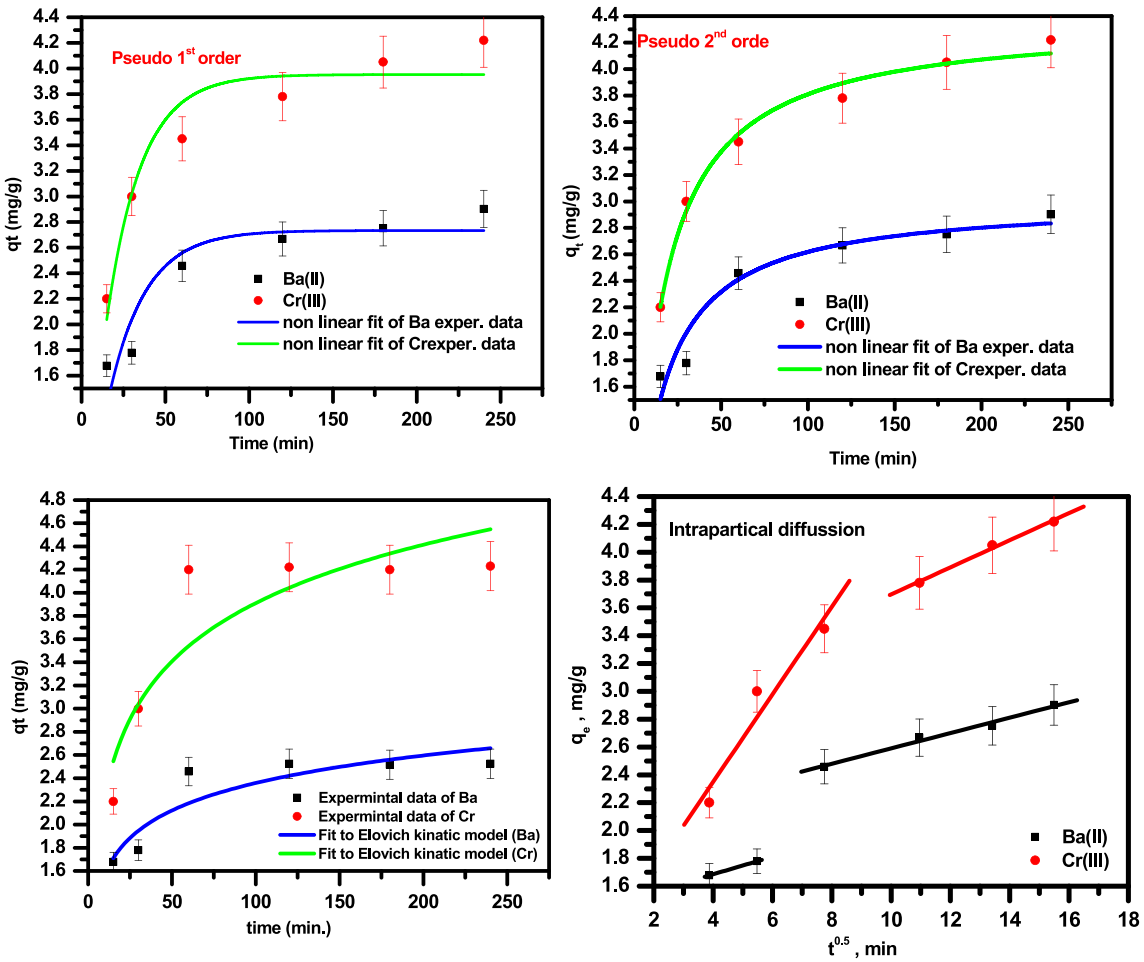

Fig. 7 Pseudo 1st order, pseudo 2nd order, Elovich, and intra-particle diffusion kinetic models plots for the adsorption of Cr(III) and Ba(II) ions onto zirconium oxide

Table 2 The parameters of the pseudo first-order and pseudo second-order kinetic models for Cr(III) and Ba(II) sorbed onto activated Zirconium oxide

Kinetic models	Parameters	Ba(II)	Cr(III)
Pseudo-first-order equation	$q_{e(exp.)}$ (mgg^{-1})	2.9	4.2
	$q_{e\ (Cal.)}$ (mgg^{-1})	2.73	3.95
	$K_1(min^{-1})$	0.045	0.048
	R^2	0.803	0.904
Pseudo-second-order equation	$q_{e\ (Cal.)}$ (mgg^{-1})	3.01	4.37
	K_2 (min^{-1})	0.022	0.015
	R^2	0.916	0.986
Intra-particle diffusion	$K_{p1}(mgg^{-1}\ min^{-1/2})$	1.43	1.09
	$K_{p2}(mgg^{-1}min^{-1/2})$	2.03	2.72
	C1	0.06	0.31
	C2	0.05	0.09
	$1R^2$	0.99	0.0.97
	$2R^2$	0.99	0.99
Elovich model	β (mg g^{-1} min^{-1})	2.919	1.370
	α (g mg^{-1})	3.34	1.54
	R^2	0.792	0.766

and Ba (II) is shown in Fig. 7. It is clear from Table 2 that the values of the correlation coefficient R^2, and the calculated adsorption capacity (q_e) are appropriate for the experimental one. These data explain that the pseudo-second order is predominant and the adsorption behavior for Cr (III) and Ba (II) is controlled by the chemical adsorption mechanism [35].

The intra-particle diffusion model elucidates the motion of ions from the bulk of the solution to the interface of an adsorbent. The Weber–Morris equation is used to interpret the intraparticle diffusion from the liquid phase into the interface of the adsorbent and can be written as the following [34]:

$$qt = K_{dis}t^{\frac{1}{2}} + C \tag{8}$$

where q_t represents to the quantity of Cr (III) and Ba(II) sorbed, K_{dis} refers to the rate constant for the intraparticle model (mg/g $min^{1/2}$), and C represents the constant that signals to the thickness of the boundary layer. The intercept of the straight curve, which is the thickness of the sorbent surface, provides information for the contribution of the adsorption onto the surface of the prepared material in the rate-determining step. As the intercept is greater, so is its contribution. Figure 7 displays the relationship between the amount of ions sorbed and $t^{1/2}$ onto the prepared zirconium oxide. It is obvious that the intra particle model for the adsorption behavior of Cr (III) and Ba (II) occurred over two stages. The first stage reports the adsorption onto the surface of the activated zirconium oxide, which may be the rate-limiting step. The second one represented equilibrium saturation. The fundamental element governing the adsorption mechanism, which includes both intra- and film diffusion, is the multi-diffusion step. Table 2 offers the parameters of this model obtained from the rate limiting step part of the linear relationship.

The parameters of non linear Elovich model can be calculated from the following Eq. 9 [36].

$$q_t = \frac{1}{\beta}Ln(1 + \alpha\beta t) \tag{9}$$

β is the initial velocity (mg g^{-1} min^{-1}) that is related to the activation energy for chemisorption and the degree of surface coverage. α is the Elovich model constant (g mg^{-1}).

From Fig. 7 and the data displayed in Table 2, it is the elucidate that the Elovich model encompasses the chemisorption of zirconium oxide towards Cr (III) and Ba (II) confirming pseudo-second order model, and this fact is similar to other studies [14, 37].

Adorption isotherms

Generally, the isotherm study is extremely helpful to interpret the parameters controlling the retention or movability of a material from the aqueous phase to a solid-adsorbent at a certain temperature and pH. A diversity of isotherm models, such as Langmuir, Freundlich and D-R models, were used to study the adsorption behavior in this work.

Langmuir isotherm model

The Langmuir isotherm model postulates that the formation of the adsorbed material onto the adsorbent is monolayer, and the adsorption can only occur at a specific number of certain limited sites, which are equivalent and identical [1, 26]. Also, this model supposes that the adsorption process is homogeneous and that all molecules have certain enthalpies and adsorption activation energies. The Langmuir nonlinear equation is written as follows [1]:

$$q_e = \frac{Q_{max}bC_e}{1 + bC_e} \tag{10}$$

where q_e represented the amount of Cr (III) and Ba (II) adsorbed at equilibrium per gram of activated zirconium oxide (mg/g), the concentration at equilibrium was symbolized by Ce (mg/l), and Q_{max} is exemplifies the monolayer adsorption capacity (mg/g), as well as b, which illustrates the constant associated with the free energy of the adsorption process.

The nonlinear fit for the Cr(III) and Ba(II) adsorption behavior onto the activated zirconium oxide sample was made clear in Fig. 8. Table 3 provides an illustration of the

model's acquired outcomes. The data in Table 3 make it clear that activated zirconium oxide's monolayer adsorption capacity (*Q*max) values for Cr (III) are significantly higher than those for Ba (II). For the adsorption process to both Cr(III) and Ba(II), the *Q*max and b constants of the Langmuir model increased as the temperature rose, showing that the capacity and intensity of adsorption are increased at higher temperatures. This raise in Q_{max} values with temperature can be interpreted as follows: the accessible active sites onto the surface of the adsorbent material increase with temperature. The visual evidence in Table 3, and Fig. 8 suggests that the adsorption of Cr (III) and Ba (II) onto activated zirconium oxide follows the Langmuir isotherm model. Additionally, other parameters, like the separation factor or

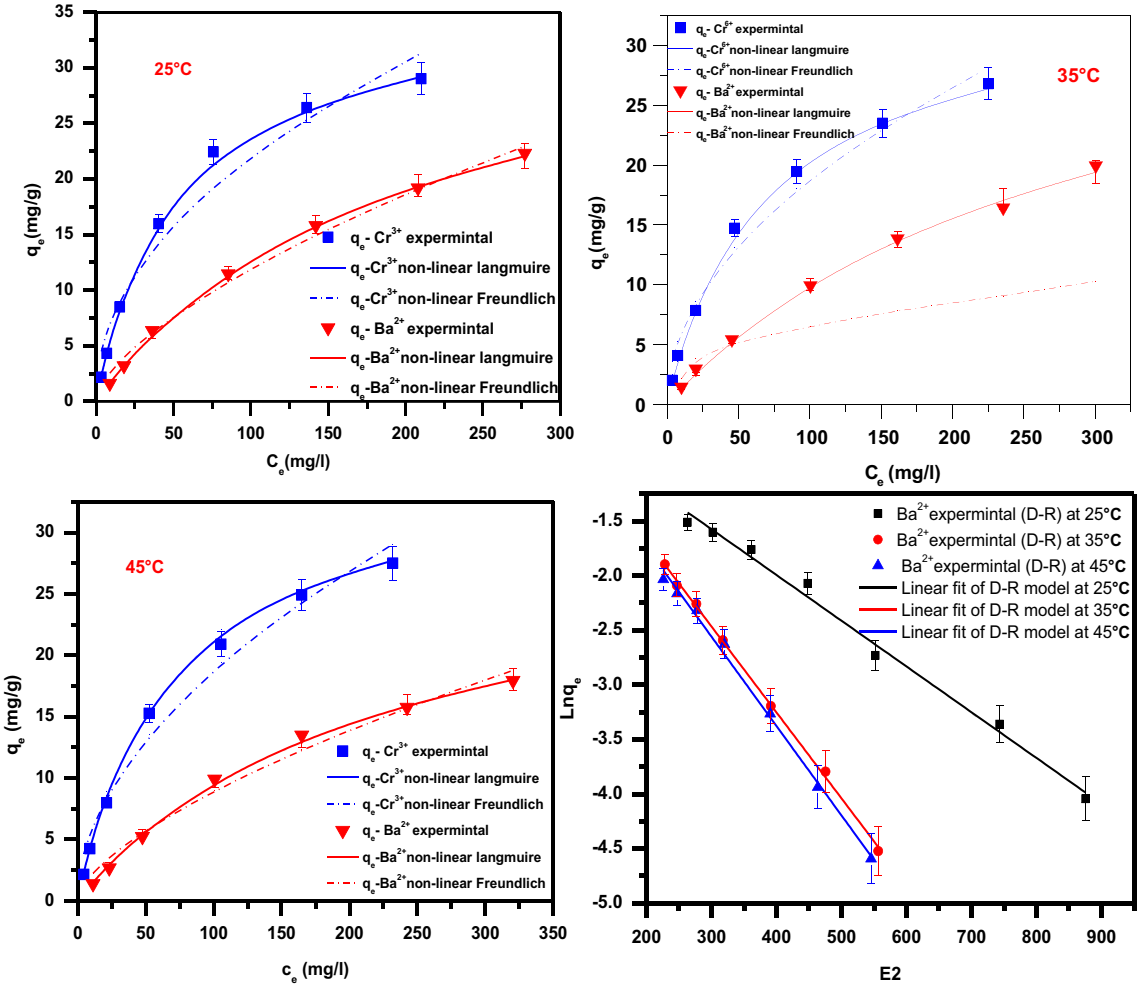

Fig. 8 Langmuir, Freundlich, and D-R isotherm plots models for the adsorption of Cr(III) and Ba(II) onto activated zirconium oxide at different temperature ranges

Table 3 Different isotherm models affection adsorption of Ba (II) and Cr (III) onto the activated zirconium oxide at different temperatures

Adsorbent	Tempe °C	Langmuir parameters				Freundlich parameters			D-R			
		q_{max} (mg/g)	b (L/mg)	R_L	R^2	1/n	k_f	R^2	q_m (mg/g)	β (mol^2 /kJ^2)	E(kJ/mol)	R^2
Cr(III)	25	35.9	0.05	0.51	0.999	2.14	2.58	0.962	121.6	0.006	8.1	0.987
	35	36.8	0.516	0.56	0.998	2.03	1.97	0.980	115.4	0.007	9.5	0.996
	45	38.2	0.912	0.63	0.994	1.96	1.79	0.979	104.5	0.007	9.8	0992
Ba(II)	25	33.9	0.045	0.81	0.999	1.57	0.64	0.994	100.1	0.004	8.2	0.991
	35	35.7	0.114	0.83	0.997	2.81	1.19	0.947	123.8	0.007	9.5	0.998
	45	36.7	0.995	0.81	0.999	1.58	0.49	0.995	124.0	0.008	11.9	0.995

the dimensionless equilibrium parameter can be determined using the Langmuir equation (R_L) [32].

$$R_L = \frac{1}{1 + bC_0} \tag{11}$$

C_o is the starting (mg/l) concentration of Cr (III) and Ba (II), respectively. If an isotherm was irreversible ($R_L = 0$), favorable ($0 > R_L < 1$), linear ($R_L = 1$), or unfavorable ($R_L > 1$), the R_L numbers indicate which type it was. Table 3 's values of R_L show that both Cr (III) and Ba (II) have favorable adsorption isotherms because they are less than 1 and greater than 0.

Freundlich isotherm model

The Freundlich isotherm depicts adsorption behavior through heterogeneous surfaces; the nonlinear form of the model can be accessed via the following equation [37]:

$$q_e = k_f C_e^{\frac{1}{n}} \tag{12}$$

C_e signifies the equilibrium concentration of Cr(III) and Ba(II), K_f signifies the relative adsorption capacity using activated zirconium oxide (mg/g), and $1/n$ signifies the model constant. Q_e represents the amount of Cr(III) and Ba(II) that was adsorbed using activated zirconium oxide. The non-linear fitting curve is shown in Fig. 8, and it is clear that the adsorption of both Cr (III) and Ba (II) onto activated zirconium oxide does not coincide with the assumptions of the Freundlich model across all concentration ranges. The various Freundlich isotherm parameters have been calculated and are shown in Table 3. The values of n determine both the heterogeneity of the adsorbent surface and the intensity of the adsorption process. The sorbent surface is expected to be more heterogeneous the closer the value is to zero; values of $1/n$ greater than one indicate chemically cooperative adsorption.

Dubinin–Radushkviech (D–R) isotherm model

In order to discuss the nature of the adsorption processes for Cr (III) and Ba (II), D-R isotherm model was also studied and written in the following form [38]:

$$\ln q_e = \ln q_m - \beta\varepsilon^2 \tag{13}$$

where q_m symbolizes the maximum amount of Cr (III) and Ba (II) that can be adsorbed onto a unit mass of activated zirconium oxide (adsorption capacity) (mmol/g), β is a constant denoting the adsorption energy (mol^2/kJ^2), ε points out the Polanyi potential $= RT \ln (1 + 1/C_e)$, R represents the gas constant (kJ/mol. K), and T refers to the absolute temperature, K. The mean free energy of adsorption has been calculated from the following:

$$E = (-2\beta)^{-\frac{1}{2}} \tag{14}$$

The value of E provides details about the adsorption mechanism, whether chemical or physical. The adsorption process is dominated by chemical mechanisms if E is between 8 and 16 kJ/mol [36]. But the adsorption mechanism is physical if the E value is less than 8.0 kJ/mol. Figure 8 shows the relationship between ln q_e and ε^2 for the adsorption of both Cr(III) and Ba(II) at various temperatures. The straight line that emerged from this relationship indicated that the D-R isotherm accurately represented the data on adsorption that had been collected. The parameters of this model are determined and displayed in Table 3. The obtained data illustrated that the values of the E for the adsorption process ranged from 8 to 16 kJ/mol, thus the mechanism of the adsorption process is chemisorption [39].

Thermodynamic studies

There are two primary ways that temperature impacts the sorption process. Elevating the temperature is recognized to accelerate the metal ion species' diffusion through the external boundary layer and into the sorbent particle's internal pores [40]. The thermodynamic parameters for the adsorption process can be estimated by computing the free energy change (ΔG^o, kJ mol^{-1}) using the following equation:

$$\Delta G^0 = -RT \ln K_{ec} \tag{15}$$

where K_{ec} is the adsorption equilibrium constant, R is the general gas constant, and T is the absolute temperature, K. ΔG^o, is the crucial quality of spontaneity. The values of K_{ec} at the studied temperatures were evaluated from the product of the Langmuir constants (Q_{max} and b) [41]. The information in Table 4 illustrates that the values of ΔG^o have a negative sign, emphasizing the spontaneous nature of the adsorption process [42]. From Eq. 16, the other parameters of thermodynamics (enthalpy change, $\Delta H°$, and entropy change, $\Delta S°$) can be calculated and tabulated in Table 4.

$$\ln K_c = \frac{\Delta S^0}{R} - \frac{\Delta H^0}{RT} \tag{16}$$

According to Eq. (16), the values of enthalpy change and entropy change can be evaluated from the slope and intercept of the straight relationship between $\ln K_{ce}$ and $1/T$, Fig. 9. The values of $\Delta H°$ are positive, which emphasizes the endothermic nature of the adsorption process, while the positive sign

Table 4 Thermodynamic parameters for the adsorption of Cr(III) and Ba(II) onto activated zirconium oxide

Temp, *K*	ΔG^{o}, kJ/mol		ΔH^{o}, kJ/mol		ΔS^{o}, J/mol.K	
	Cr(III)	Ba(II)	Cr(III)	Ba(II)	Cr(III)	Ba(II)
298	−6.70	−5.79	114.2	112.9	390.2	381.7
313	−33.73	−16.88				
333	−42.26	−41.25				

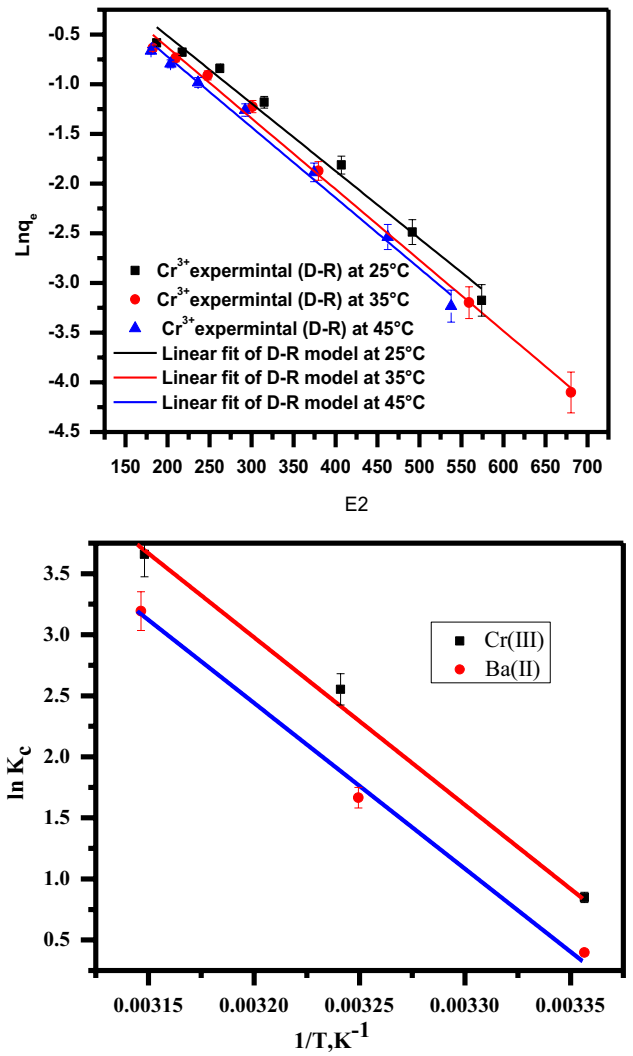

Fig. 9 Thermodynamic study for the adsorption of Cr(III) and Ba(II) onto activated zirconium oxide at different temperature ranges

of ΔS° indicates the growth in randomness at the activated zirconium oxide/solution interface through the adsorption process.

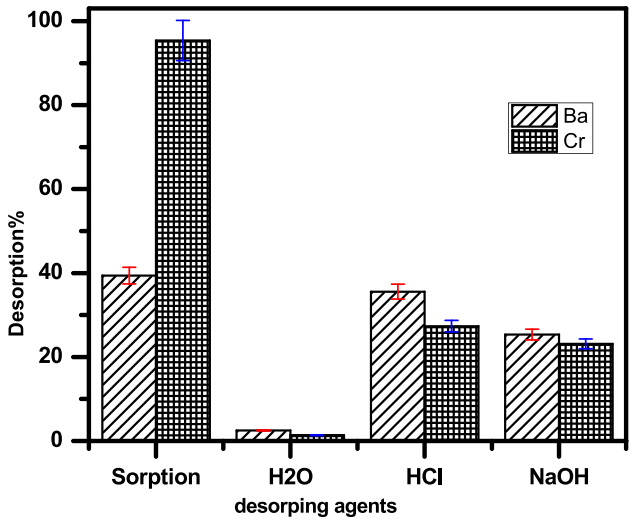

Fig. 10 Effect of different desorbing agents (0.1 M HCl, 0.1 M NaOH, and H_2O) on the regeneration of zirconium oxide loaded with Ba(II) and Cr(III)

Desorption study

The effectiveness of an adsorbent in treating wastewater is contingent upon its capacity for absorption as well as its propensity for regeneration [43]. Also improving process economics is probably going to be largely dependent on the sorbent's regeneration [44]. As displayed in Fig. 10, the desorption efficiency of acid (0.1 M HCl) is better than that of base (0.1 M NaOH) and water. So, HCL is more favorable as a desorbing agent than NaOH and water for the regeneration and reuse of zirconium oxide. From Fig. 10, HCL (0.1 M) shows desorption of Cr (III), and Ba (II), with desorption efficiency of 30% and 37%, respectively.

Effect of interfering ions

The effect of several competing ions, such as Zn (II), Ca (II), and Na (I) on the elimination of Cr(III) and Ba(II) from the prepared activated zirconium oxide has been studied (Fig. 11). A certain weight of prepared sorbent material (0.1 g) and different concentrations of Zn (II), Ca

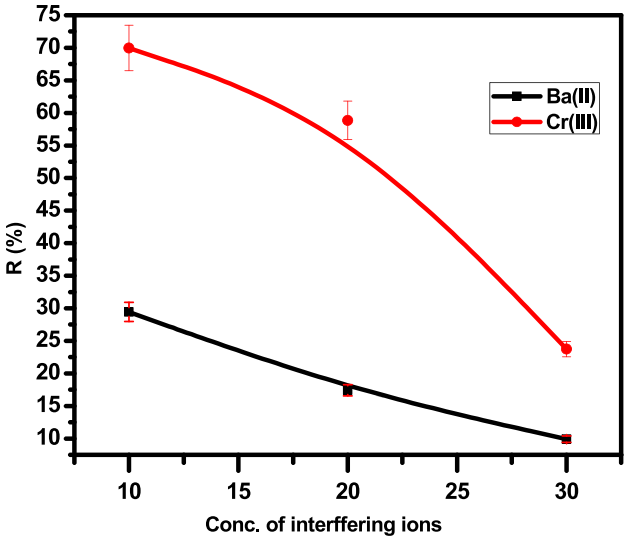

Fig. 11 Effect of different concentration (10,20, and 30 mg/l) interfering ions Zn (II), Ca(II), and Na(I) on the removal % of Cr(III) and Ba(II) onto zirconium oxide (Ci of Ba(II) and Cr (III) = 50 mg/l, v = 10 ml, pH = 5, and 2 h shaking time)

(II), and Na (I) (10, 20, and 30 ppm), as well as Cr (III) and Ba (II) (50 ppm), have been mixed at optimum conditions of pH and temperature. In Fig. 11, it is obvious that the percent uptake of Cr (III) and Ba (II) decreased with an increase in the concentration of competing ions. The notable negative influence of interfering ion concentrations may be attributed to the interaction of the competing ions with the surface of zirconium oxide. The factor that may have an effect on the adsorption of both ions is the ion radius [45]. Ions with a small ionic radius may be adsorbed onto the surface of the sorbent, and they penetrate the pores faster than the other ions. The ionic radius of Na(I) (0.95°A), Ca (II) (1.00°A), and Zn(II) (1.42°A) has a smaller ionic radius than Ba (II) (2.35°A) and Cr (III) (1.66°A). This indicates that the smallest ionic radius could be adsorbed onto the pores of activated zirconium oxide material; therefore, the adsorption of Cr (III) and Ba (II) is decreased.

Comparison the sorption capacity

The obtained sorption capacity of the prepared material has been compared with that of other materials, as seen in Table 5.

Table 5 comparison the maximum capacity of Ba(II) and Cr(III) with other adsorbent

Material	Saturated sorption capacity (mg/g)		References
	Cr(III)	Ba(II)	
Chorfa silt material	26.30	NR	[46]
Zinc ferrite-humic acid nanocomposite	NR	63.33	[47]
Spent coffee waste biochars	NR	6.17	[48]
Pecan shell based activated carbon	NR	3.33	[49]
SP(M) (miswak powder)	NR	34.97	[50]
Chitosan-sodium alginate hydrogels	48.0	NR	[51]
Carboxymethyl cellulose-g-poly(acrylic acid-co-acrylamide)	47.7	NR	[52]
Starch-craft-itaconic acid hydrogels	14.13	NR	[53]
Caboxymethyl cellulose S2	NR	9.28	[54]
Activated zirconium oxide	35.9	33. 9	Present work

Reaction mechanism

An important substance having acid–base properties, zirconium dioxide (ZrO_2) is extremely stable in both oxidizing and reducing environments. Metal cations (Zr) serve as Lewis acids or potential electron charge acceptors, whereas O^-_2 anions serve as conjugated bases. The nature of the acidic and basic sites, as well as their quantity and acidity/base strength, all have an impact on the selectivity of many reactions. At least five stable structural polymorphs of zirconia exist, each with unique characteristics. At low temperatures, the monoclinic ZrO_2 phase (m-ZrO_2) is stable. On the surface of m-ZrO_2, there are eight distinct oxygen atoms. O_1 to O_5 are surface-bound, but O_6 to O_8 are subsurface-bound and are unable to bind the metal cation under study [53].

Nagaoka et al. reported that several bonding models of metal ions and zirconia have been proposed. M^+ is adsorbed onto the zirconia surface via hydrogen bonding between the M–O^- and Zr–OH groups. The second model indicates that M^+ may interact with zirconia via ionic bonding [54].

Conclusion

Synthetic activated zirconium oxide was tested as an inorganic sorbent for removal of Cr (III) and Ba (II) from aqueous solution. The kinetics of both Cr (III) and Ba (II) were studied, and the obtained results were analyzed using four kinetic models. Results explained that the pseudo second order adsorption mechanism is predominant, and the overall rate constant of adsorption behavior for Cr (III) and Ba (II) appears to be controlled by the chemical adsorption process. Equilibrium isotherms have been determined and tested

for different isotherm expressions, and the adsorption data were successfully modeled using Langmuir, Freundlich, and Dubinin-Radushkviech (D-R) approaches. Based on the D-R model expression, the maximum adsorption capacity and the mean free energy of the studied ions have been determined. The adsorption of Cr (III) and Ba (II) is an endothermic process and spontaneous in nature. The surface of the loaded ZrO is more regenerated using Hcl (0.1 M) than NaOH and H_2O. The *R%* decreased as the concentration of interfering ions increased.

Data and material availability

All authors are sure that all data and materials, as well as software applications or custom code, support the published claims and comply with field standards.

Author contribution Maha A. Youssef (first author) was responsible for the measurement of the batch sorption study and the analysis of the data, writing, review, and editing. These measurements and their analyses were conducted in the Hot Laboratories and Waste Management Center- Egyptian Atomic Energy Authority. Abeer EL khalafawy (second author) contributed to the formal analysis, investigation, data curation, and review of the original draft. Hisham S. Hassan was responsible for conceptualization, supervision, visualization, and reviewing the original draft.

Funding The authors declare that no funds, grants, or other support were received during the preparation of this manuscript.

Declarations

Conflict of interest The authors declare no conflict of interest.

Ethical approval The submitted manuscript is original and hasn't been published elsewhere in any form or language.

Consent to publication All authors agreed with the content and gave explicit consent to submit, and we obtained consent from the responsible authorities (the Egyptian atomic energy authority where the work has been carried out) **before** the work was submitted.

References

1. Hassan HS, Abdel Moamen OA, Zaher AWF (2020) Neuro-Fuzzy inference system analysis on sorption studies of strontium and cesium cations onto a novel impregnated nano-zeolite. Adv Powd Techn 31:1125–1139
2. Khorasgani MD, Faghihian H, Givianrad MH, Azar PA, Tehrani MS (2022) Synthesis and application of a novel mesoporous SBA-15 sorbent functionalized by 2,4 dinitrophenyl hydrazine (DNPH) for simultaneous removal of Pb(II), Cr(III), Cd(II) and Co(II) from aqueous solutions: experimental design, kinetic, thermodynamic, and isotherm aspects. Adv Powd Techn 33:103201
3. Dakroury G, Abo-Zahra SF, Hassan HS, Ali HEA (2020) Improvement of the sorption behavior of aluminum silicate composite toward ^{134}Cs and ^{60}Co radionuclides by non-living biomass of *Chlorella vulgaris*. Environ Sci Pollu Res 27:21109–21125
4. Zhang J, Yan M, Sun G, Liu K (2021) Simultaneous removal of Cu(II), Cd(II), Cr(VI), and rhodamine B in wastewater using TiO_2 nanofibers membrane loaded on porous fly ash ceramic support. Separ Purifi Technol 272:118888
5. Abdulkhair B, Salih M, Modwi A, Adam F, Elamin N, Seydou M, Rahali S (2021) Adsorption behavior of barium ions onto ZnO surfaces: experiments associated with DFT calculations. J Mol Struct 1223:128991
6. Majidnia Z, Idris A, Abd Majid M, Zin RM, Ponraj M (2015) Efficiency of barium removal from radioactive waste water using the combination of maghemite and titanium nanoparticles in PVA and alginate beads. Appl Radit Isotope 05:105–113
7. Fontana KB, Chaves ES, Kosera VS, Lenzi GG (2018) Barium removal by photo- catalytic process: an alternative for water treatment. J Water Process Eng 22:163–171
8. Kanwar VS, Sharma A, Srivastav AL, Rani L (2020) Phytoremediation of toxic metals present in soil and water environment: a critical review. Environ Sci Pollut Res 27:44835–44860
9. Prasad S, Yadav KK, Kumar S, Gupta N, Cabral-Pinto MMS, Rezania S, Radwan N, Alam J (2021) Chromium contamination and effect on environmental health and its remediation: a sustainable approaches. J Environ Manage 285:112174
10. Park JE, Shin JH, Oh W, Choi S-J, Kim J, Kim C, Jeon J (2022) Removal of hexavalent chromium(VI) from wastewater using chitosan-coated iron oxide nanocomposite *membranes*. Toxics 10(2):98. https://doi.org/10.3390/toxics10020098
11. Vital B, Bartacek J, Ortega-Bravo JC, Jeison D (2018) Treatment of acid mine drainage by forward osmosis: heavy metal rejection and reverse flux of draw solution constituents. Chem Eng J 332:85–91
12. Hargreaves AJ, Vale P, Whelan J, Alibardi L, Constantino C, Dotro G, Cartmell E, Campo P (2018) Impacts of coagulation-flocculation treatment on the size distribution and bioavailability of trace metals (Cu, Pb, Ni, Zn) in municipal wastewater. Water Res 128:120–128
13. Chen Q, Liang S, Zhang H, Liu D, Zhuo L (2021) Fabrication and characterization of W-Ni nanocomposites via a facile chemical co-precipitation route. Adv Powder Technol 32(3):908–915
14. Attallah MF, Hassan HS, Youssef MA (2019) Synthesis and sorption potential study of Al_2O_3-ZrO_2-CeO_2 composite material for removal of some radionuclides from radioactive waste effluent. Appl Radiat Isotop 147:40–47
15. Hassan HS, Elmaghraby EK (2019) Retention behavior of cesium radioisotope on poly (acrylamido-sulfonicacid) synthesized by chain polymerization. Appl Radiat Isot 146:40–47
16. Fawzy MA (2020) Biosorption of copper ions from aqueous solution by Codium Vermilara Optimization, kinetic, isotherm and thermodynamic studies. Adv Powder Technol 31:3724–3735
17. Li R, Zhai Z, Li Y, Yang T, Chen Y (2018) Kinetic study of heavy metals Cu and Zn removal during sewage sludge ash calcination in air and N_2 atmospheres. J Hazard Mater 347:227–232
18. Sanad MMS, Farahat MM, Abdel Khalek MA (2021) One-step processing of low cost and superb natural magnetic adsorbent: kinetics and thermodynamics investigation for dye removal from textile wastewater. Adv Powd Technol 32:1573–1583
19. Shahrivar J, Gharabaghi M (2020) Separation of $AuCN_2$-by activated carbon and functionalized graphene/activated carbon composite. Adv Powd Technol 31:4648–4656
20. Li J, Hui L, Zhang W, Lu J, Yang Y, Feng H (2021) Scalable production of ultra small TiO_2 nano crystal/activated carbon composites by atomic layer deposition for efficient removal of organic pollutants. Adv Powd Technol 32:728–739
21. Dalmieda J, Kruse P (2019) Metal cation detection in drinking water. Sensors 19(3):5134

22. Hassan HS, Attia LA, Dakroury GA (2020) Exploration of the parameters affecting the radioactive europium removal from aqueous solutions by activated carbon-epoxy composite. Appl Radit Isotop 164:109278
23. Mahmoud ME, Saad EA, El-Khatib AM, Soliman MA, Allam EA (2017) Adsorptive removal of Zn(II), Co(II) and their radioactive isotopes ^{65}Zn, ^{60}Co on the surface of sodium nano bentonite coated with oleyl-amine. J Rad Nucl Appl 2(3):87–93
24. Dakroury GA, Abo-Zahra SF, Hassan HS, Fathy NA (2020) Utilization of silica–chitosan nanocomposite for removal of $^{152+154}$Eu radionuclide from aqueous solutions. J Radioanalyt Nucl Chem 323:439–455
25. K. Simeonidis K, Martinez-Boubeta C, Zamora-Perez P, Rivera-Gil P, Kaprara E, Kokkinos E, Mitrakas M (2018) Nanoparticles for heavy metal removal from drinking water. In: Environ Nanotech, Springer, 75–124.
26. Abdel Maksoud MIA, Sami NM, Hassan HS, Bekhit M, Ashour AH (2022) Novel adsorbent based on carbon-modified zirconia/spinel ferrite nanostructures: evaluation for the removal of cobalt and europium radionuclides from aqueous solutions. J Coll Interf Sci 607:111–124
27. Abdel Moamen OA, Hassan HS, El-Sherif EA (2017) Binary oxide composite adsorbent for copper, nickel and zinc cations removal from aqueous solutions. Desalin Water Treat 82:219–233
28. Liu X, Pang H, Liu X, Li Q, Zhang N, Mao L, Qiu M, Hu B, Yang H, Wang X (2021) Orderly porous covalent organic frameworks-based materials: superior adsorbents for pollutants removal from aqueous solutions. Innovation 2:100076
29. Dakroury GA, Ali SM, Hassan HS (2021) Assessment of adsorption performance of chitosan/ZrO_2biosorbent composite towards Cs (I) and Co (II) metal ions from aqueous solution. J Polym Res 28:385
30. Zhang X, Zhang M, Zhang J, Zhang Q, Tsubaki N, Tan Y, Han Y (2019) Methane decomposition and carbon deposition over Ni/ZrO_2 catalysts: comparison of amorphous, tetragonal, and monoclinic zirconia phase. Int J Hydrogen Energy 44(33):17887–17899
31. Aziz SB, Karim W, Brza M, Abdulwahid R, Raza SS, Al-Zangana S, Kadir M (2019) Ion transport study in CS: POZ based polymer membrane electrolytes using trukhan model. Int J Mol Sci 20(21):5265
32. Hassan HS, Madcour W, Elmaghraby EK (2019) Removal of radioactive cesium and europium from aqueous solutions using activated Al_2O_3 prepared by solution combustion. Mater Chem Phys 234:55–66
33. Chinchamalatpure VR, Chore SM, Patil SS, Chaudhari GN (2012) Synthesis and electrical characterization of ZrO_2 Thin films on Si(100). J Mod Phys 3(1):69–73. https://doi.org/10.4236/jmp.2012.31010
34. Deng J, Lid S, Xiong L, Jiao Y, Yuan S, Wang J, Chen Y (2020) Preparation of nanostructured CeO_2-ZrO_2-based materials with stabilized surface area and their catalysis in soot oxidation. Appl Surf Sci 505:144301
35. Sharaf G, Hassan H (2014) Removal of copper ions from aqueous solution using silica derived from rice straw: comparison with activated charcoal. Int J Environ Sci Technol 11:1581–1590
36. Ho Y-S, McKay G (1999) Pseudo-second order model for sorption processes. Process Biochem 34:451–465. https://doi.org/10.1016/S0032-9592(98)00112-5
37. Dakroury GA, Abo-Zahra ShF, Hassan HS (2020) Utilization of olive pomace in nano MgO modification for sorption of Ni(II) and Cu(II) metal ions from aqueous solutions. Arab J Chem 13:6510–6522
38. Abdel Maksoud MIA, Sami NM, Hassan HS, Awed AS (2021) Sorption characteristics of bismuth tungstate nanostructure for removal of some radionuclides from aqueous solutions. Sep Purifi Technol 277:119478
39. Yang T, Wang Y, Sheng L, He C, Sun W, He Q (2020) Enhancing Cd(II) sorption by red mud with heat treatment: performance and mechanisms of sorption. J Environ Manag 255:109866
40. El-khalafawy A, Imam DM, Youssef MA (2022) Enhanced biosorption of europium and cesium ions from aqueous solution onto phalaris seed peel as environmental friendly biosorbent: equilibrium and kinetic studies. Appl Radiat Isotopes 190:110498
41. Panayotova MI (2001) Kinetics and thermodynamics of copper ions removal from wastewater by use of zeolite. Waste Manag 21:671–676
42. Bayramoglu G, Arica MY (2017) Polyethylenimine and tris(2-aminoethyl)amine modified p(GA–EGMA) microbeads for sorption of uranium ions: equilibrium, kinetic and thermodynamic studies. J Radioanal Nucl Chem 312(2):293–303. https://doi.org/10.1007/s10967-017-5216-z
43. Arica MY, Bayramoglu G (2016) Polyaniline coated magnetic carboxymethylcellulose beads for selective removal of uranium ions from aqueous solution. J Radioanal Nucl Chem 310(2):711–724. https://doi.org/10.1007/s10967-016-4828-z
44. Erkaya IA, Arica MY, Akbulut A, Bayramoglu G (2014) Biosorption of uranium(VI) by free and entrapped *Chlamydomonas reinhardtii*: kinetic, equilibrium and thermodynamic studies. J Radioanal Nucl Chem 299(3):1993–2003. https://doi.org/10.1007/s10967-014-2964-x
45. Youssef MA, Attia LA (2023) Novel nano *Rosmarinus officinalis* phytomass adsorbent for strontium and europium removal from aqueous solution: batch and packet techniques. J Radioanal Nucl Chem 332:1935–1952. https://doi.org/10.1007/s10967-023-08862-z
46. Ouadjenia-Marouf F, Marouf R, Schott J, Yahiaoui A (2013) Removal of Cu(II), Cd(II) and Cr(III) ions from aqueous solution by dam silt. Arab J Chem 11:401–406
47. Abdel Maksoud MIA, Murad GA, Zaher WF, Hassan HS (2023) Adsorption and separation of Cs(I) and Ba(II) from aqueous solution using zinc ferrite-humic acid nanocomposite. Sci Rep 13:5856
48. Jaegwan S, Jinwoo K, Yong-Gu L, Sangwon K, Changgil S (2021) Changes in adsorption mechanisms of radioactive barium, cobalt, and strontium ions using spent coffee waste biochars via alkaline chemical activation: enrichment effects of O-containing functional groups. Environ Res 199:111346
49. Kaveeshwar AR, Kumar PS, Revellame ED, Gang DD, Zappi ME, Subramaniam R (2018) Adsorption properties and mechanism of barium(II) and strontium(II) removal from fracking wastewater using pecan shell-based activated carbon. J Cleaner Prod 20:1–13
50. Hassan SSM, Kamel AH, Youssef MA, Aboterika AHA, Awwad NS (2020) Removal of barium and strontium from wastewater and radioactive wastes using a green bioadsorbent, *Salvadora persica* (Miswak). Desalin Water Treatm 192:306–314
51. Guan X (2022) Remediation and resource utilization of chromium(III)-containing tannery effluent based on chitosan-sodium alginate hydrogel. Carbohydr Polym 284:119179
52. Fei, Y, Deng, H, Wu, G, Luo, M, Chen, Y, Wang, X, Ye, H, Liu, T (2022) Insight into adsorption process and mechanisms of Cr(III) using carboxymethyl cellulosegpoly(acrylic acid-co-acrylamide)/attapulgite composite hydrogel. Environ Technol. 1–51
53. Alexis S, Ranjan R, Andrew G, Jason R, Marie J (2023) Selective adsorption of Cr(III) over Cr(VI) by starch-graft-itaconic acid hydrogels. J Hazard Mater Adv 10:100255
54. Abass MR, Youssef MA, Eid MA (2023) Inorganic composites based on carboxymethyl cellulose: preparation, characterization, sorption, and selectivity behavior for some radionuclides from radioactive solutions. Radiochim Acta. https://doi.org/10.1515/ract-2023-0214
55. Maleki F, Pacchioni G (2020) Characterization of acid and basic sites on zirconia surfaces and nanoparticles by adsorbed probe

molecules: a theoretical study. Top Catal 63:1717–1730. https://doi.org/10.1007/s11244-020-01328-6
56. Nagaoka N, Yoshihara K, Feitosa V et al (2017) Chemical interaction mechanism of 10-MDP with zirconia. Sci Rep 7:45563. https://doi.org/10.1038/srep45563